Journal of Computational Physics **157,** 327–349 (2000)
doi:10.1006/jcph.1999.6385, available online at http://www.idealibrary.com on IDEAL®

# Double Fourier Series on a Sphere: Applications to Elliptic and Vorticity Equations

Hyeong-Bin Cheong

*Department of Environmental Atmospheric Sciences, Pukyong National University, 599-1 Daeyeon-3-dong Nam-gu, Pusan 608-737, Korea*

Received September 28, 1998; revised April 12, 1999

The solution of elliptic and vorticity equations on a sphere is studied using double Fourier series as orthogonal basis functions. The basis functions incorporate sine series weighted by cosine latitude as meridional basis functions for even zonal wavenumbers other than zero to meet the pole condition. As to the solution of Poisson's equation, it is found that the new method gives improved accuracy compared to the method of Yee (*Mon. Weather Rev*. **109**, 501, 1981) due to the absence of constraints imposed on spectral coefficients with the operation number being slightly increased. The new method is applied to the vorticity equation along with the use of Fourier and spherical harmonics filters, and its accuracy is tested for the rotated Rossby–Haurwitz wave. It is shown that the basis functions adopted here provide high accuracy for all tests used. Numerical integration without spherical harmonics filters indicates that they are necessary for stable and accurate time integration. Comparison with the spherical harmonics model reveals that the present method is more accurate by a factor of order $1\frac{1}{2}$ for the test case. Further application to the advection equation is carried out. The error measure for the strong advection of the cosine bell with various rotation angles indicates that the present method is capable of producing accurate and stable calculations without the pole problem, suggesting that it could be applied to the numerical weather prediction model, including shallow water equations, without difficulty. Extension to the shallow water equations with accuracy tests as in Williamson *et al*. (*J. Comput. Phys*. **102**, 211, 1992) will be given in the future. Additional time could be saved by introducing the reduced grids near poles in the present method, besides the advantage of applying FFT to both longitudinal and latitudinal directions. 

*Key Words:* double Fourier series; elliptic equation; Poisson equation; spectral method; spherical-harmonics filter; vorticity equation.



0021-9991/00 $35.00

## 1. INTRODUCTION

The use of double Fourier series in solving partial differential equations (PDEs) is an attractive method because in addition to its high accuracy, a fast algorithm is available when transforming from the wave to the grid domain and vice versa. Double Fourier series in spectral or pseudospectral method for the global atmospheric models has emerged as an alternative to the spherical harmonics method in an attempt to reduce the complexity and the computational cost that is primarily caused by the use of Legendre functions [2, 4, 17, 21, 23]. Nevertheless, most global atmospheric models use the spherical-harmonics-based spectral method [9, 15, 27]. Reasons for this may be found in [5]. Recently, a stable and accurate pseudospectral method in which double Fourier series are used was developed by [24] based on the method of [17].

When double Fourier series are incorporated as basis functions in spectral methods for the solution of PDEs in a spherical coordinate system, one must be careful that the boundary condition at the poles is satisfied. Such a condition, however, is not necessary for the pseudospectral method as used by Merilees [17] and Spotz *et al*. [24] because $2\pi$-periodicity is used on great circle meridian. One way to overcome this is to select basis functions that satisfy the pole condition [23]. Another way is to impose a constraint on spectral coefficients when each basis function does not satisfy the pole condition [2, 4, 21]. Since spherical harmonics are represented as proper combinations of half-ranged cosine or sine series, one naturally tries to use double Fourier series expansions that are appropriate for the representation of spherical harmonics [4, 7, 8, 21, 26]. Such basis functions do not necessarily satisfy the pole condition.

The Poisson equation on a spherical surface appears in a variety of problems. A number of numerical methods for its solution have been published [1, 6, 18, 21, 25, 31, 32]. It often serves as an important method of testing whether a certain kind of basis function can be adopted in a spectral method for PDEs. Since spherical harmonics are eigenfunctions of the Laplacian operator, the most accurate solution of the Poisson equation may be obtained by the use of these functions even for higher order equations such as the biharmonic equation. However, such a solution requires larger computations as the resolution increases.

Yee [32] presented the solution of the Poisson equation using double Fourier series on a spherical surface. The basis functions were sine (cosine) series for odd (even) zonal wavenumbers, which were used originally by Orszag [21], though not in explicit expressions,

$$g_m(\phi) = \sum_{n=0}^{\infty} g_{n,m}\{(1-s)\cos n\phi + s \sin n\phi)\},$$

where $\phi$ is latitude $+\pi/2$ so that the zero of $\phi$ is taken at the south pole, $g_m$ is the Fourier transform of $g(\lambda, \phi)$, and $s = 0$ $(s = 1)$ for even (odd) zonal wavenumber $m$, respectively (in fact, the colatitude was used in [32] instead of $\phi$). Use of the cosine function makes it necessary to impose a constraint on spectral coefficients for even zonal wavenumbers except zero because it does not vanish at the poles. In principle, the basis functions above cannot be applied to differential equations involving advection terms on a shpere for two reasons: First, the singularity from the factor $(1/\sin\ \phi)$ is unavoidable or may be treated inefficiently. Second, any spectral components representing a physical quantity should be determined by the governing equation in use, but not by the necessity of the pole condition itself.

An example of the application of double Fourier series to an advection equation on a sphere is found in [2], where interior grids are used to avoid singularity over the poles and the meridional basis functions are defined over a great circle passing over the poles. Since the basis functions do not satisfy the pole condition, it is required that the sum of odd (or even) coefficients for the meridional function should vanish. However, it is questionable whether this requirement must be fulfilled during time integration.

In this study, we present a double Fourier series method for the solution of simple elliptic equations, the vorticity and advection equations, on a sphere based on interior grids in an attempt to provide the first step for the application to a numerical weather prediction model including the shallow water equations. The new method is similar to Yee's method [32] in that double Fourier series with half-ranged sine or cosine series for meridional direction are used, but the basis functions are different from Yee's. In previous studies including [32], double Fourier expansion on a sphere (half-ranged functions in meridional direction) incorporates explicitly cosine series for even zonal wavenumbers [4, 21]. We also use a cosine series, but in implicit expression. That is, for even zonal wavenumbers except zero we expand dependent variables with sine series weighted by cosine latitude, which makes it unnecessary to impose a constraint on spectral coefficients in order to satisfy the pole condition.

In the next section the solution of elliptic equations including the Poisson equation on a sphere using double Fourier series is described. Section 3 shows the application of the new method to the vorticity and advection equations with test cases incorporating the Rossby–Haurwitz wave and the advection of a cosine bell, respectively. Comparisons with other methods, as in [15, 28], are also presented. Discussion and conclusions are given in the final section.

## 2. POISSON EQUATION ON A SPHERE

### 2.1. *Basis Functions and Poisson Equation*

The Poisson equation over a sphere with unit radius is written as

$$\frac{1}{\sin\phi}\frac{\partial}{\partial\phi}\sin\phi\frac{\partial u}{\partial\phi}+\frac{1}{\sin^2\phi}\frac{\partial^2 u}{\partial\lambda^2}=g(\lambda,\phi), \tag{2-1}$$

where $\lambda$ is longitude and $\phi$ is defined as in Section 1 (see also Boer and Steinberg [2]); $g(\lambda,\phi)$ is the forcing function given. As a usual procedure, we expand the field variables with a Fourier series in longitude with a truncation $M$, e.g.,

$$u(\lambda,\phi)=\sum_{m=-M}^{M}u_m(\phi)e^{im\lambda}, \tag{2-2}$$

where $i=\sqrt{-1}$, $u_m(\phi)$ is the complex Fourier coefficient given by

$$u_m(\phi)=\frac{1}{K}\sum_{k=0}^{K-1}u(\lambda_k,\phi)e^{-im\lambda_k}, \tag{2-3}$$

and $\lambda_k = 2\pi k/K$ and $K$ is the number of data points along a latitude circle. To make the transforms in (2-2) and (2-3) complete, we set $2M = K$. Then, we obtain

$$\frac{1}{\sin\phi}\frac{d}{d\phi}\sin\phi\frac{d}{d\phi}u_m(\phi) - \frac{m^2}{\sin^2\phi}u_m(\phi) = g_m(\phi), \tag{2-4}$$

where $g_m(\phi)$ is the complex Fourier coefficient of $g(\lambda, \phi)$.

Without loss of generality, the boundary conditions at the poles for the Fourier coefficients of any analytic true scalar functions, e.g., $g_m(\phi)$, can be imposed:

$$\begin{aligned} g_m(\phi) &= \begin{cases} \text{finite}, & m = 0 \\ 0, & m \neq 0 \end{cases} \\ \frac{d}{d\phi}g_m(\phi) &= \begin{cases} \text{finite}, & \text{odd } m \\ 0, & \text{even } m. \end{cases} \end{aligned} \tag{2-5a,b,c,d}$$

These are classified as the essential boundary conditions for the Laplacian operator [4]. The basis functions for spectral representation in the meridional direction should satisfy these conditions. It is clear that the use of either sine or cosine series alone as basis functions does not meet the boundary conditions above. If the basis functions do not satisfy the pole conditions, additional constraints are required [2, 21, 31, 32]. In this study we approximate $g_m(\phi)$ (and $u_m(\phi)$) with the truncated sine or cosine functions

$$\begin{aligned} g_0(\phi) &= \sum_{n=0}^{J-1} g_{n,0}\cos n\phi, && m = 0 \\ g_m(\phi) &= \sum_{n=1}^{J} g_{n,m}\sin n\phi, && \text{odd } m \\ g_m(\phi) &= \sum_{n=1}^{J} g_{n,m}\sin^l\phi\sin n\phi, && \text{even } m\ (\neq 0). \end{aligned} \tag{2-6a,b,c}$$

Any positive integer of $l$ will be appropriate for the pole conditions written above. With $l \geq 2$, the cosine series can also satisfy the pole condition. However, since with large $l$ the round-off error becomes large for the inverse transform [11], we select the minimum value of $l$, i.e., $l = 1$. Equations (2-6a) and (2-6b) are identical to those used in previous studies [4, 21, 32]. Explicit use of the cosine series for even $m$ requires the imposition of a condition that the sum of expansion coefficients should vanish [4, 21, 32]. With the basis functions in (2-6), however, this is not the case.

We assume that the field variables are given on interior grids in the latitudinal direction,

$$\begin{aligned} g_m(\phi) &= g_m(\phi_j) \\ \phi_j &= \pi(j + 0.5)/J, \qquad j = 0, 1, 2, \ldots, J-1, \end{aligned} \tag{2-7a,b}$$

where $J$ is the total number of grid points between poles. With this grid location we do not have to deal directly with the grid points on the poles, and thus, we can avoid the singularity arising from dividing by $\sin\phi$ in the case of even $m$ ($\neq 0$), which is needed to take advantage of the fast sine transform. Evaluation of any terms (e.g., the advection terms, as will be seen in the next section) that include the operation of $1/\sin\phi$ is also possible over the sphere. The spectral coefficients $g_{n,m}$ are calculated by either sine or cosine transforms on interior

grids with a fast algorithm found in Press *et al*. [22],

$$
\begin{aligned}
g_{n,m} &= \frac{b}{J}\sum_{j=0}^{J-1} g_m(\phi_j)\cos(n\phi_j/J), && m=0,\\
g_{n,m} &= \frac{c}{J}\sum_{j=0}^{J-1} g_m(\phi_j)\sin(n\phi_j/J), && \text{odd } m,\\
g_{n,m} &= \frac{c}{J}\sum_{j=0}^{J-1} (g_m(\phi_j)/\sin\phi_j)\sin(n\phi_j/J), && \text{even } m\ (\neq 0),
\end{aligned}
\tag{2-8a,b,c}
$$

where $b=1$ for $n=0$ and $b=2$ for $n>0$, $c=1$ for $n=J$ and $c=2$ for $n<J$. The procedure for obtaining the solution of (2-4) is basically similar to that of Yee [32]. However, some differences are found between the two procedures; these arise partly from the difference in basis functions and partly from the choice of interior grids.

### 2.2. *Spectral Representation for Odd* $\boldsymbol{m}$

Multiplication by $\sin^2\phi$ and substitution of the Fourier expansion (2-6b) into (2-4) yields

$$
\begin{aligned}
&\frac{(n-1)(n-2)}{4}u_{n-2,m} - \frac{n^2+2m^2}{2}u_{n,m} + \frac{(n+1)(n+2)}{4}u_{n+2,m}\\
&\quad = -\frac{1}{4}g_{n-2,m} + \frac{1}{2}g_{n,m} - \frac{1}{4}g_{n+2,m},
\end{aligned}
\tag{2-9}
$$

where $n=2,4,\ldots,J$ for even $n$, and $n=1,3,\ldots,J-1$ for odd $n$. Discarding the expansion coefficients with indices higher than the truncation limit, Eq. (2-9) constitutes two matrix equations for each $m$, with even or odd $n$, separately,

$$
D\mathbf{u} = A\mathbf{g}, \tag{2-10}
$$

where $D$ and $A$ are square matrices of $J/2\times J/2$ with tridiagonal components only whose values are calculated by the coefficients in (2-9). $\mathbf{u}$ and $\mathbf{g}$ are column vectors whose components are the expansion coefficients of $u_m(\phi)$ and $g_m(\phi)$. As to a particular index, it holds that

$$
A_{1,1} = 3/4 \qquad \text{for odd } n, \tag{2-11}
$$

where $g_{-1,m} = -g_{1,m}$ was used due to the $2\pi$-periodicity of $g_m(\phi)$.

### 2.3. *Spectral Representation for Even* $\boldsymbol{m}$ $(\neq 0)$

Equation (2-4) is rewritten with transformed variables $g_m^{\mathrm{s}}$ and $u_m^{\mathrm{s}}$ ($g_m^{\mathrm{s}} \equiv g_m/\sin\phi$, $u_m^{\mathrm{s}} \equiv u_m/\sin\phi$) as

$$
\left(u_m^{\mathrm{s}}\right)''\sin^2\phi + \frac{3}{2}\left(u_m^{\mathrm{s}}\right)'\sin 2\phi + u_m^{\mathrm{s}}\cos 2\phi = g_m^{\mathrm{s}}\sin^2\phi, \tag{2-12}
$$

where the prime denotes differentiation with respect to $\phi$. Substitution of Eq. (2-8c) yields algebraic equations similar to (2-9),

$$
\frac{n(n-1)}{4}u_{n-2,m} - \frac{n^2+2m^2}{2}u_{n,m} + \frac{n(n+1)}{4}u_{n+2,m} = -\frac{1}{4}g_{n-2,m} + \frac{1}{2}g_{n,m} - \frac{1}{4}g_{n+2,m}, \tag{2-13}
$$

where $n = 1, 3, \ldots, J-1$ ($n = 2, 4, \ldots, J$) for odd (even) $n$. Again, this can be rewritten in matrix equations such as (2-10). For the same reason stated above, the matrix component for a particular index is given as

$$A_{1,1} = 3/4 \qquad \text{for odd } n.$$

### 2.4. *Spectral Representation for* $\boldsymbol{m} = 0$

Linear algebraic equations exactly the same as (2-9) can be obtained with the use of expansion coefficients, but this time $n = 0, 2, \ldots, J-2$ for even $n$, and $n = 1, 3, \ldots, J-1$ for odd $n$. It is trivial from (2-9) to show that $D_{1,1} = D_{2,1} = 0$ for even $n$. Matrix components that should not follow the coefficients in (2-9) are

$$\begin{aligned} A_{1,1} &= 1/4 \qquad \text{for odd } n \\ A_{2,1} &= -1/2 \qquad \text{for even } n, \end{aligned}$$

where $g_{-1,0} = g_{1,0}$ was used for the first equation, and the second identity comes from

$$\begin{aligned} g_0(\phi)\sin^2\phi \equiv Z_0(\phi) &= \sum_{n=0}^{J-1} g_{n,0}\cos n\phi \frac{1-\cos 2\phi}{2} \\ \therefore Z_{2,0} &= -\frac{1}{2}g_{0,0} + \frac{1}{2}g_{2,0} - \frac{1}{4}g_{4,0}. \end{aligned}$$

From direct substitution of (2-6a) into (2-4) it is clear that we must discard $g_{-2,0}$ and $u_{-2,0}$ in (2-9) so that we have $A_{1,2} = -1/4$ and $D_{1,2} = 1/2$.

### 2.5. *Tests of the Method*

To get the solution of $u(\lambda_k, \phi_j)$ from given $g(\lambda_k, \phi_j)$, we may follow the procedure shown in Yee [32]. First we obtain the spectral components of the forcing function $g_m(\phi_j)$ by Fourier transforms in longitude. Prior to the Fourier transform in latitude, a variable transform such as $g_m(\phi_j)/\sin\phi_j$ is carried out, and then the spectral coefficients $g_{n,m}$ are calculated. We next solve the matrix equations as in (2-10): The right-hand side is first calculated to get a column vector, i.e., $\mathbf{Z} = A\mathbf{g}$. Finally the tridiagonal matrix equation $D\mathbf{u} = \mathbf{Z}$ is solved. Since the matrix elements $D_{1,1} = D_{2,1} = 0$ for $m = 0$ and even $n$, $u_{0,0}$ may have an arbitrary constant. The tridiagonal systems are calculated very efficiently by prehandling the matrices just once to facilitate backward substitution in a Gaussian elimination procedure. In our method an extra procedure that is not found in Yee [32] is needed to get $g_m(\phi_j)/\sin\phi_j$ for even $m$ ($\neq 0$), which occurs twice. This requires only $2 \times J \times M$ operations, which is just a small percentage of the total number of operations involved in the entire procedure. In test calculations, we select $J$ to be an integer power of 2 to take full advantage of the FFT algorithm, and determine $K = 2J$ giving the same resolution in longitude and latitude. Referring to Yee [32], we see that the total number of operations needed to get $u(\lambda_k, \phi_j)$ from given $g(\lambda_k, \phi_j)$ on regular grids (i.e., not interior grids) is $12J^2(1 + \log_2 J)$ with this grid number. Therefore if $J = 128$ is given, the number of operations in the new method exceeds that in Yee [32] by about 2%.

To test the accuracy of the new method and to give a direct comparison with the previous study, we introduce a function whose analytic solution is known,

$$
\begin{aligned}
g(\lambda,\phi) &= g^a + g^b,\\
g^a &= \begin{cases} (m+1)(m+2)\cos\phi\sin^m\phi\cos m(\lambda - d_m) & \text{for } m>0\\ 2\cos\phi & \text{for } m=0 \end{cases}\\
g^b &= \begin{cases} m(m+1)\sin^m\phi\cos m(\lambda - e_m) & \text{for } m>0\\ -2(1+3\cos 2\phi) & \text{for } m=0, \end{cases}
\end{aligned}
\tag{2-14}
$$

where $d_m$ and $e_m$ are random phases ranging from 0 to $2\pi$. The exact solution for this is

$$
\begin{aligned}
u(\lambda,\phi) &= u^a + u^b,\\
u^a &= \begin{cases} \cos\phi\sin^m\phi\cos m(\lambda - d_m) & \text{for } m>0\\ -\cos\phi & \text{for } m=0 \end{cases}\\
u^b &= \begin{cases} \sin^m\phi\cos m(\lambda - e_m) & \text{for } m>0\\ +\cos 2\phi & \text{for } m=0. \end{cases}
\end{aligned}
\tag{2-15}
$$

The function $g^a$ ($g^b$) is antisymmetric (symmetric) about the equator, denoting the first antisymmetric (symmetric) mode of associated Legendre function with the zonal wavenumber $m$. To see the dependence of the accuracy of the calculations on spatial resolution, $J$ is given as 16, 32, 64, and 128, which correspond to the grid numbers $32\times 16$, $64\times 32$, $128\times 64$, and $256\times 128$, respectively.

In the computation all the variables were set to be in double precision for which floating points of 15 digits were available (DIGITAL FORTRAN 90 was used on DIGITAL UNIX Alpha systems). For a direct comparison with the new method, we also carried out the same computation using Yee's method. As a measure of accuracy we calculated the normalized $L^2$ error $E$ over the globe defined by

$$
E^2 = \frac{\sum_k \sum_j \left(u_{k,j} - u^A_{k,j}\right)^2}{\sum_k \sum_j \left(u^A_{k,j}\right)^2}, \tag{2-16}
$$

where $u_{k,j}$ and $u^A_{k,j}$ denote the calculated and analytic solutions on grid points. In Fig. 1 we show the result $\log_{10} E$ for various resolutions, where all calculations were repeated 30 times with different sets of random phases, $d_m$ and $e_m$, and averaged. It is noted that the magnitude of error exhibits a fluctuation with a zonal wavenumber whose amplitude reaches approximately one order. At fixed resolution and $m$ the error remains on the same order for both the present (denoted by M16, M32, M64, and M128) and Yee's method (Y16, Y32, Y64, and Y128). As it should be, there exist no significant differences in error for odd $m$ because the basis functions are the same. As a whole, however, the present method is more accurate than Yee's method for even $m$, typically by a factor of several times, in the case of high resolutions ($128\times 64$ and $256\times 128$ grids). This difference is attributed to the fact the basis functions as in (2-6c) satisfy the pole condition (2-5d) and thus do not need the constraint imposed on spectral coefficients used in Yee's method. For both methods, accuracy increases at fixed $m$ in direct relation to resolution, except for low wavenumbers, for which accuracy slowly decreases with increased resolution.

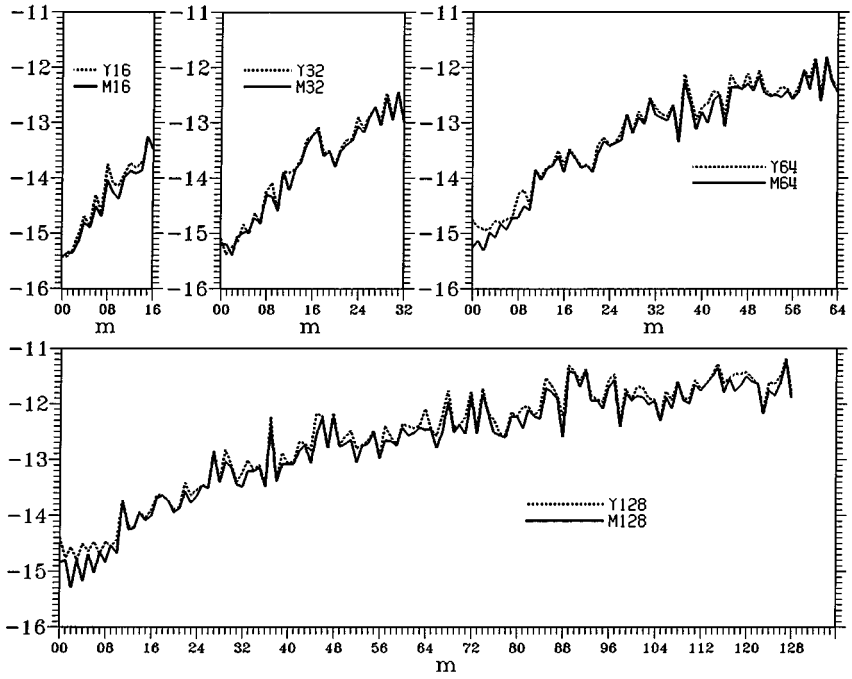


**FIG. 1.** Variation of $\log_{10} E$ with zonal wavenumbers for various resolutions. Dashed (solid) line denotes the result of Yee's method (new method).

### 2.6. *Extension to Simple Elliptic Equations*

It may be possible to extend the present method to the solution of other simple types of elliptic equations on a sphere. One such equation is the Helmholtz equation, which frequently occurs in a variety of problems:

$$\nabla^2 u - \varepsilon u = g(\lambda, \phi). \tag{2-17}$$

With $\varepsilon = 0$, Eq. (2-17) becomes the same as Eq. (2-1). In this case the global integral of the forcing function does not necessarily vanish. With some manipulation, Eq. (2-17) is written as the matrix equation

$$F\mathbf{u} = A\mathbf{g}, \qquad F = D - \varepsilon A. \tag{2-18a,b}$$

The same procedure as stated above can be applied to the solution of the column vector **u**. Unlike in Eq. (2-10), $u_{0,0}$ is determined uniquely in the case of $\varepsilon \neq 0$.

A second example is the biharmonic equations [6], whose general form may be written as

$$(\nabla^2 - \varepsilon)\nabla^2 u = g(\lambda, \phi). \tag{2-19}$$

This can be solved with ease if we introduce an intermediate variable $w = \nabla^2 u$. It should be remembered that integration of the forcing function over the globe vanishes for this problem. As noted by Dennis and Quartapelle [6], the accuracy of the solution is subject to the magnitude of $\varepsilon$. To investigate the dependence of the accuracy on $\varepsilon$ for the new

**TABLE I**
**Normalized Error for Biharmonic Equation of Helmholtz–Poisson Type with $m = 32$ ($K \times J = 128 \times 64$)**

| $\log_{10} \varepsilon$ | $E$ |
|---|---|
| 4 | 0.259986E−12 |
| 3 | 0.385253E−12 |
| 2 | 0.219036E−11 |
| 1 | 0.179361E−10 |
| 0 | 0.764823E−10 |
| −1 | 0.108322E−09 |
| −2 | 0.106658E−09 |
| −3 | 0.944021E−10 |

method, $\varepsilon$ is set to vary over a range of several orders. For the evaluation of accuracy, the forcing function in Eq. (2-19) is given to satisfy Eq. (2-19) when $u$ is given as in Eq. (2-15). The results with $K \times J = 128 \times 64$ and $m = 32$ are summarized in Table I. Note that the accuracy does not change significantly until $\varepsilon$ increases to $O(1)$, but increases sharply in the interval of $\varepsilon \approx O(10^1)$–$O(10^3)$. That is, as the relative magnitude of the fourth order term becomes more important, accuracy decreases. In fluid dynamics including numerical weather prediction models [14], fourth order Helmholtz–Poisson-type equations (i.e., Eq. (2-19)) frequently appear. In such problems, the parameter $\varepsilon$ is generally very large (or the second order term is relatively important) so that the degradation of accuracy may not be a serious problem. The accuracy remains almost the same as that for the Poisson equation.

Until now our interest has been focused on the solution of simple elliptic equations such as Poisson, Helmholtz, and biharmonic equations when the forcing function is known. In various problems the solution of the forcing function of the examples shown above, i.e., the result of operations of the Laplacian operator, is needed. First consider obtaining $g(\lambda, \phi)$ from $u(\lambda, \phi)$ in Eq. (2-1). For this purpose the left-hand side of Eq. (2-10) is first calculated using the spectral components $u_{n,m}$ to get a column vector $\mathbf{Z}(=D\mathbf{u})$, and $A\mathbf{g} = \mathbf{Z}$ is solved for column vector $\mathbf{g}$.

Harmonic equations of orders higher than biharmonic are commonly found as a viscosity term in numerical models with spectral method [16], e.g., $\nabla^6 u$, $\nabla^8 u$. These equations are also easily calculated by introducing an intermediate variable to yield a Poisson-type equation. Note that just one variable transform such as $u_m(\phi_j)/\sin\phi_j$ is required for the evaluation of the fourth order equations as well as even higher order equations when we want to obtain spectral coefficients of these from given $u(\lambda, \phi)$.

## 3. VORTICITY EQUATION AND SPECTRAL REPRESENTATION

### 3.1. *Model Equation and Spectral Forms*

The nondivergent barotropic vorticity equation on a sphere scaled by the radius $a$ and the inverse of rotation rate $\Omega^{-1}$ of the earth is written

$$\frac{\partial \zeta}{\partial t} = -\frac{U}{\sin^2\phi}\frac{\partial \eta}{\partial \lambda} - \frac{V}{\sin\phi}\frac{\partial \eta}{\partial \phi}, \tag{3-1}$$

with the definitions of the variables as

$$\begin{aligned} \eta &= \zeta + f, \\ \zeta &= \nabla^2 \psi, \\ U &\equiv u \sin\phi = -\sin\phi \frac{\partial \psi}{\partial \phi}, \\ V &\equiv v \sin\phi = \frac{\partial \psi}{\partial \lambda}, \end{aligned} \tag{3-2a,b,c,d}$$

where $f$ is the Coriolis parameter and $u$ and $v$ represent the zonal and meridional velocities, respectively. Equation (3-1) contains one prognostic variable, $\zeta$, and three diagnostic variables, $\psi, U$, and $V$, that can be determined directly from the vorticity. We represent the vorticity field as the sum of basis functions with wavenumber truncations $M$ and $N$ for zonal and meridional directions, respectively (one more meridional component is included in zonal mean state):

$$\begin{aligned} \zeta(\lambda, \phi, t) &= \sum_{m=-M}^{M} \zeta_m(\phi, t) e^{im\lambda} \\ \zeta_m(\phi, t) &= \begin{cases} \sum_{n=0}^{N} \zeta_{n,m}(t) \cos n\phi & \text{for } m = 0, \\ \sum_{n=1}^{N} \zeta_{n,m}(t) \sin n\phi & \text{for odd } m, \\ \sum_{n=1}^{N} \zeta_{n,m}(t) \sin\phi \sin n\phi & \text{for even } m\ (\neq 0). \end{cases} \end{aligned} \tag{3-3a,b,c,d}$$

One must be careful in applying the parity function $\sin\phi$ and/or differentiation with respect to $\phi$ to a true scalar function, say $\psi(\lambda, \phi)$. Only certain combinations of differential operators and parity functions are allowed to avoid the Gibbs phenomenon at the poles, of which some examples are

$$\begin{aligned} &\tfrac{\partial^q \psi}{\partial \phi^p} \sin^p\phi; \qquad p + q = 0, \pm 2, \ldots, \qquad \text{and} \qquad q = 1, 2, \ldots, \\ &\psi \sin^p \phi; \qquad p = \pm 2, \pm 4, \ldots. \end{aligned} \tag{3-4}$$

Thus the use of $U$ and $V$ instead of $u$ and $v$, respectively, is for more reasons than to deal with simpler forms. Further, all terms included in (3-1) may be classified as one of these forms.

The spectral components $\zeta_{n,m}$ are obtained by half-ranged cosine or sine transforms, which can be written in integral forms (see Eq. (2-8) for discrete forms)

$$\zeta_{n,m}(t) = \begin{cases} \frac{b}{\pi} \int_0^\pi \zeta_m(\phi, t) \cos n\phi \, d\phi & \text{for } m = 0 \\ \frac{2}{\pi} \int_0^\pi \zeta_m(\phi, t) \sin n\phi \, d\phi & \text{for odd } m \\ \frac{2}{\pi} \int_0^\pi \{\zeta_m(\phi, t) / \sin\phi\} \sin n\phi \, d\phi & \text{for even } m\ (\neq 0) \end{cases} \tag{3-5}$$

with $b = 1$ for $n = 0$ and $b = 2$ for $n > 0$. The spectral components for the stream function are found by solving tridiagonal matrix equations as described in Section 2. Let zonal Fourier components of $U(\lambda, \phi, t)$ and $\psi(\lambda, \phi, t)$ be $U_m(\phi, t)$ and $\psi_m(\phi, t)$, respectively; then, the

spectral form of the velocities is

$$U_{n,m} = \begin{cases} n\{\psi_{n+1,m} - \psi_{n-1,m}\}/2 & \text{for even } m \neq 0 \\ \{(n+1)\psi_{n+1,m} - (n-1)\psi_{n-1,m}\}/2 & \text{for others} \end{cases}$$
$$V_{n,m} = im\psi_{n,m}, \tag{3-6a,b,c}$$

where

$$U_m^{\mathrm{s}} \equiv U_m/\sin\phi = -\sin\phi\frac{\partial}{\partial\phi}\psi_m^{\mathrm{s}} - \psi_m^{\mathrm{s}}\cos\phi$$
$$\left(\psi_m^{\mathrm{s}} \equiv \psi_m/\sin\phi\right) \tag{3-7}$$

is used for even $m\,(\neq 0)$. In an analogous manner, we may relate the spectral form of $\eta_\lambda\,(\equiv\frac{\partial\eta}{\partial\lambda})$ and $\eta_\phi\,(\equiv\sin\phi\frac{\partial\eta}{\partial\phi})$ to that of $\eta$. We must keep the meridional truncation for $U_{n,m}$ and $(\eta_\phi)_{n,m}$ one level above that for the stream function and absolute vorticity $\eta$, respectively. The spectral components of nonlinear terms are evaluated by the transform method [2, 3, 20]. We get grid-point values of $U$, $V$, $\eta_\lambda$, and $\eta_\phi$ by inverse transform and calculate the nonlinear products such as $U\eta_\lambda/\sin^2\phi$ and $V\eta_\phi/\sin^2\phi$, finally transforming them into spectral components $X_{n,m}$ and $Y_{n,m}$, respectively. Note that only $O(M^2\log_2 K)$ operations are needed for each transform due to the availability of FFT, while $O(MN^2)$ are needed for the spectral harmonics model [3, 20]. Then, the spectral form of the vorticity equation (3-1) is written as

$$\frac{d}{dt}\zeta_{n,m} = -X_{n,m} - Y_{n,m}. \tag{3-8}$$

The spectral equation does not require a necessary condition for the spectral components used in [2] because the basis functions satisfy the pole condition. The basis functions in (3-3) make the spectral representation more accurate and simpler than for any other Fourier method ever used.

The integration of a function over the sphere may be derived in the spectral form (cf. Boer and Steinberg [2]). Let $[g]$ denote the global average of a function $g(\lambda,\phi)$:

$$[g] \equiv \frac{1}{4\pi}\int_0^{\pi}\int_0^{2\pi} g(\lambda,\phi)\sin\phi\,d\lambda\,d\phi. \tag{3-9}$$

Expansion of $g(\lambda,\phi)$ with basis functions yields

$$[g] = \frac{1}{2}\int_0^{\pi}\left[\sum_{n=0}^{N} g_{n,0}\cos n\phi\sin\phi\right]d\phi$$
$$= \sum_{n=0}^{N/2}\frac{g_{2n,0}}{1-(2n)^2}, \tag{3-10}$$

where $g_{n,m}$ are the spectral coefficients. Integration of nonlinear products such as enstrophy and kinetic energy may be done by the transform method: Nonlinear products are evaluated on grid points and the zonal component is transformed into the spectral domain to use (3-10). Although many more operations are needed than this, nonlinear products can also

be calculated directly from spectral components,

$$[gq] = \sum_{m\ \text{odd}} \sum_{n} \sum_{n'} \frac{1}{2}(g_{n,m}q^*_{n,m} + \text{c.c.})S_o(n,n') + \sum_{n} \sum_{n'} \frac{1}{2}(g_{n,o}q^*_{n,o} + \text{c.c.})S_w(n,n')$$
$$+ \sum_{\substack{m\ \text{even} \\ (\neq 0)}} \sum_{n} \sum_{n'} \frac{1}{2}(g_{n,m}q^*_{n,m} + \text{c.c.})\left\{\frac{1}{2}S_o(n,n') + S_e(n,n')\right\},$$

where the asterisk and c.c. mean the complex conjugate and

$$S_o(n,n') = \left\{\frac{n}{n^2-(n'-1)^2} - \frac{n}{n^2-(n'+1)^2}\right\}$$
$$S_w(n,n') = \frac{1}{2}\left\{\frac{n'+1}{(n'+1)^2-n^2} - \frac{n'-1}{(n'-1)^2-n^2}\right\}$$
$$S_e(n,n') = \frac{1}{4}\left\{\frac{n'}{n'^2-(n-1)^2} - \frac{n'}{n'^2-(n+1)^2}\right\} - \frac{1}{4}\left\{\frac{n}{n^2-(n'-3)^2} - \frac{n}{n^2-(n'+3)^2}\right\}$$

with $n \pm n' =$ even.

Since from (3-1) the global integral of the vorticity is conserved over time, the spectralized equations should also satisfy this conservation property. Equation (3-8), however, does not explicitly show the conservation of the vorticity. Nevertheless, the vorticity is conserved to a very good approximation during time integration, as will be shown below. On the other hand, if Eq. (3-1) is written in flux form, the corresponding spectral equations explicitly show the conservation of the vorticity, which is illustrated in the Appendix. We found that the spectral form in (3-8) gives more accurate results for the test than does that in (A-4).

### 3.2. *Truncation and Fourier Filter*

Given the zonal and meridional truncation $M$ and $N$, the number of grid points in longitude ($K$) and latitude ($J$) should be determined sufficient to prevent the aliasing error:

$$K \geq 3M + 1, \qquad J \geq (3N+1)/2. \tag{3-11a,b}$$

In this problem, we set $M = N$ (as will be seen later, $N$ must be not greater than $M$) and choose the total grid points to satisfy (see Table II for resolutions and number of grid points)

$$K = 4M, \qquad J = 2N. \tag{3-12}$$

The transform grid points are located on the even positions in longitude, but along the

**TABLE II**
**Grid Numbers for Various Resolution**

| | $K$ | $J$ | $M$ | $N$ |
|---|---|---|---|---|
| M16 | 64 | 32 | 16 | 16 |
| M32 | 128 | 64 | 32 | 32 |
| M64 | 256 | 128 | 64 | 64 |

*Note.* $K(J)$ is total grids in the zonal (meridional) direction, and $M(N)$ is the maximum zonal (meridional) wavenumber.

interior grid in latitude as in Section 2, which facilitates the meridional transform of any function including the $(1/\sin\phi)$ factor.

When spherical coordinates are used as in (3-1), a severe limitation on the size of the time step arises from the decrease of zonal grid size as the poles are approached. The zonal resolution increases with latitude by the factor $(1/\sin\phi)$; therefore the resolution near the poles is almost $M$ times better than that at the equator. This inefficiency and severe difference in resolution can be overcome by discarding higher zonal wavenumbers near the poles [2, 12, 17, 24]. There are various ways to accomplish this. In this study, we restrict the largest zonal wavenumber retained to be

$$\min(M^c, M), \qquad M^c = 6 + (M - 6)\sin\phi. \tag{3-13}$$

This is done at every time step. With this filtering at least six zonal components are retained at the grid points nearest to the poles; correspondingly we have a zonal resolution at the poles approximately six times better than that at the equator. If the equal resolutions are provided at the poles and the equatorial region ($M^c = M\sin\phi$), almost all of the Rossby–Haurwitz waves may be wrongly represented by making the amplitude zero near poles.

In addition to the applicability of FFT for both longitudinal and latitudinal directions, this model has the important advantage that the reduction of zonal grids at high latitudes is also possible as in the spherical-harmonics-based spectral model [12], which cannot be realized in the pseudospectral model [17, 24].

### 3.3. *Spherical Harmonics Filter*

The eigensolutions of the linearized equation of (3-1) without zonal mean flow represent the Rossby–Haurwitz waves [11], whose spatial structures are the same as those of the spherical harmonics. The phase speed of Rossby–Haurwitz waves is expressed as $-2/n(n+1)$, where $n$ is an integer denoting the total wavenumber. With the double Fourier series as the basis functions, a limited number of eigensolutions are exact for $m \geq 3$, while all eigensolutions are exact for $m < 3$. At any time, the vorticity field can be expressed as the sum of these eigensolutions. From these we must filter out the incorrect eigensolutions from the total field to maintain the accuracy and stability of the long-term numerical integration.

To calculate the eigenmodes of the linearized equation of (3-1) we expand the vorticity using the basis functions in (3-3) with a meridional truncation $N$ and let $\zeta_{n,m}(t) = \hat{\zeta}_{n,m}\exp(-i\sigma t)$. Then we get an eigensystem with a spectral components base,

$$B\hat{\boldsymbol{\zeta}} = \hat{\sigma}\hat{\boldsymbol{\zeta}}, \tag{3-14}$$

where $B = D^{-1}A$ and $\hat{\sigma} = \sigma/2m$, and $\hat{\boldsymbol{\zeta}}$ represents a column vector of $N/2$ components for both even and odd modes. The eigensystem is solved by the use of Mathematica [30] for various resolutions. In Table III, the normalized error calculated for selected wavenumbers is illustrated. We confirmed that only the first $N_e$ modes are correct where $N_e$ is given as

$$\begin{aligned} &M/2 - (|m| - 2)/2 \qquad \text{for even } m \\ &M/2 - (|m| - 1)/2 \qquad \text{for odd } m. \end{aligned}$$

Thus, we must take the zonal truncation to be not less than the meridional truncation, i.e., $N \leq M$ in the present model.

**TABLE III**
**Normalized Error of Eigenvalues for Zonal Wavenumbers 3, 4, and 16**

| $n$ | $m=3$ (odd) | $m=3$ (even) | $m=4$ (odd) | $m=4$ (even) | $m=16$ (odd) | $m=16$ (even) |
|---|---|---|---|---|---|---|
| 1 | −0.18E−14 | 0.41E−15 | −0.55E−15 | 0.45E−14 | 0.23E−15 | −0.53E−15 |
| 2 | −0.20E−15 | −0.26E−14 | 0.29E−15 | 0.36E−14 | −0.29E−15 | 0.82E−15 |
| 3 | −0.77E−15 | 0.19E−14 | 0.62E−15 | 0.15E−15 | −0.72E−15 | −0.26E−14 |
| 4 | 0.18E−14 | −0.19E−15 | 0.40E−14 | −0.11E−15 | −0.15E−14 | 0.35E−15 |
| 5 | −0.80E−15 | 0.10E−14 | 0.13E−15 | 0.20E−14 | −0.13E−14 | 0.28E−15 |
| 6 | −0.31E−15 | 0.72E−15 | 0.72E−15 | 0.00E+00 | −0.16E−14 | −0.98E−15 |
| 7 | −0.41E−15 | 0.58E−15 | −0.10E−14 | −0.13E−15 | −0.70E−15 | 0.15E−14 |
| 8 | 0.10E−14 | 0.14E−14 | 0.22E−14 | 0.41E−14 | 0.00E+00 | 0.21E−15 |
| 9 | 0.23E−14 | 0.91E−15 | 0.54E−15 | −0.16E−14 | −0.45E−15 | 0.24E−15 |
| 10 | 0.60E−15 | 0.10E−14 | 0.30E−14 | 0.26E−14 | 0.93E−03 | 0.10E−02 |
| 11 | −0.71E−15 | −0.13E−14 | 0.52E−15 | 0.35E−14 | 0.21E−01 | 0.23E−01 |
| 12 | 0.15E−14 | −0.24E−14 | 0.24E−14 | 0.13E−14 | 0.10E+00 | 0.11E+00 |
| 13 | −0.32E−14 | 0.17E−14 | 0.17E−15 | 0.75E−15 | 0.27E+00 | 0.28E+00 |
| 14 | 0.75E−15 | 0.10E−14 | −0.18E−14 | 0.21E−14 | 0.50E+00 | 0.50E+00 |
| 15 | 0.25E−15 | 0.68E−15 | 0.91E−15 | 0.85E−15 | 0.73E+00 | 0.74E+00 |
| 16 | 0.22E+00 | 0.22E+00 | 0.45E+00 | 0.45E+00 | 0.92E+00 | 0.92E+00 |

*Note.* The left column denotes the mode number, and "odd" and "even" imply the symmetric and antisymmetric modes with respect to the equator. $n$ represents the $n$th mode of the eigensolution.

The detailed procedure for applying the spherical-harmonics filter to the vorticity field in the case of odd modes (hemispherically symmetric modes) is illustrated. We first solve the linear system

$$\begin{aligned} Q\mathbf{a} &= \boldsymbol{\zeta} \\ \boldsymbol{\zeta} &\equiv \{\zeta_{1,m}, \zeta_{3,m}, \ldots, \zeta_{N-1,m}\}^T \\ \mathbf{a} &\equiv \{a_1, a_3, \ldots, a_{N-1}\}^T, \end{aligned} \tag{3-15a,b,c}$$

where $Q$ is an $N/2 \times N/2$ matrix consisting of the eigenvectors. After $\mathbf{a}$ is obtained, it is made $a_n = 0$ for the last $N_e$ solutions. Then filtered coefficients for the vorticity are calculated with the operation of the left-hand side of (3-15a). It should be remembered that the filtering actually selects the wave components relevant to the triangular truncation for the spherical-harmonics-based spectral model.

The number of operations required to apply the spherical-harmonics filter once is approximately. $MN^2$ ($LU$ decomposition of $Q$ is done only once), which is much larger than that needed for the evaluation of nonlinear terms $O(N^2 \log_2 J)$.[1] So, to keep the advantage coming from the FFT unharmed by the application of the spherical-harmonics filter, it is desirable to use it less frequently than every $O(M/\log_2 J)$ time steps. This corresponds to one application every several tens of time steps even for very high resolution, e.g., $M = 512$. As will be shown later, such less frequent use proves to be sufficient for the prevention of numerical instability. Moreover, stability is not so sensitive to the small change in frequency.

[1] Since the advantage of the double Fourier series model lies in the significant enhancement of efficiency for the meridional transform, the operation counts should be compard for the meridional direction.

### 3.4. *Tests with Rossby–Haurwitz Waves*

In this section, we use the rotated, stable Rossby–Haurwitz wave [13] for tests. The Coriolis parameter and the initial relative vorticity are given as

$$\begin{aligned} f(\lambda', \theta') &= 2\sin\theta' \\ \zeta(\lambda', \theta') &= 2r\sin\theta' + rn(n+1)\cos^4\theta'\sin\theta'\cos 4\lambda', \\ r &\equiv 2/\{n(n+1)-2\} \end{aligned} \tag{3-16a,b,c}$$

where $n = m + 1$ with $m = 4$. $\lambda'$ and $\theta'$ are defined as

$$\begin{aligned} \sin\theta' &= R_{xz}\sin(\gamma+\alpha) \\ \tan\lambda' &= \frac{\cos\theta\sin\lambda}{R_{xz}\cos(\gamma+\alpha)} \\ R_{xz} &= (\cos^2\theta\cos^2\lambda + \sin^2\theta)^{1/2} \\ \gamma &= \arctan\left(\frac{\tan\theta}{\cos\lambda}\right), \end{aligned} \tag{3-17a,b,c,d}$$

with $\theta$ being the latitude and $\alpha$ representing the rotation angle of the earth axis. This corresponds to a stationary Rossby–Haurwitz wave of $(n, m) = (5, 4)$ mode superimposed on the basic flow of superrotation (the first term on the right-hand side of (3-16b)). As $\alpha$ increases to $\pi/2$, the flow over the poles becomes stronger. $\alpha$ very close to $\pi/2$ will be the most severe test because it contains the asymmetry between the east and west hemispheres. The stream function and $u$ obtained from (3-16b) with the rotation angle $\alpha = \pi/2 - 0.05$ are illustrated in Fig. 2. The error estimates are

$$\begin{aligned} L_2 &= \frac{\left[(u-u_T)^2 + (v-v_T)^2\right]^{1/2}}{\left[u_T^2 + v_T^2\right]^{1/2}} \\ L_3 &= \frac{\max\left\{(u-u_T)^2 + (v-v_T)^2\right\}^{1/2}}{\max\left\{u_T^2 + v_T^2\right\}^{1/2}}, \end{aligned} \tag{3-18a,b}$$

where the square brackets denote the global average. $u$ and $v$ are thevelocities on grid

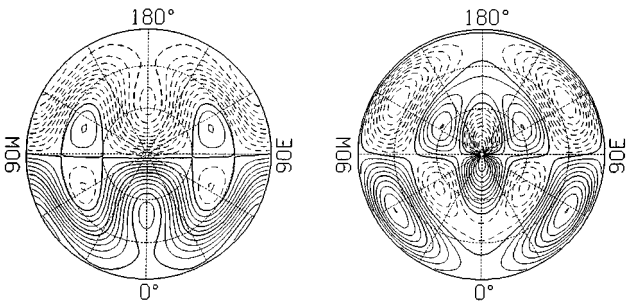


**FIG. 2.** Initial fields of stream function (left) and $\boldsymbol{u}$-velocity (right) with contour interval of $10^7$ m$^2$ s$^{-1}$ and 10 m s$^{-1}$, respectively, in the case of $\alpha = \pi/2 - 0.05$. Positive (negative) values are in solid (dashed) lines, and latitudinal circles and meridians are drawn every 30°. Only the northern hemisphere is shown.

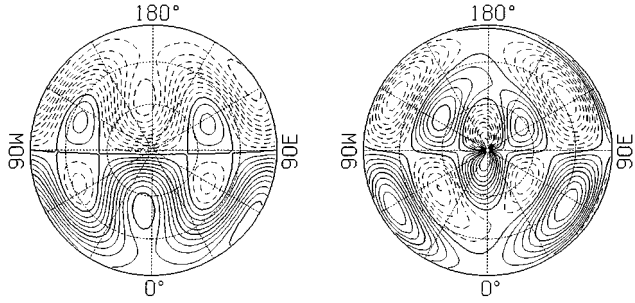


**FIG. 3.** Fields of stream function (left) and $\boldsymbol{u}$-velocity (right) at 64.5 h with $\alpha = \pi/2 - 0.05$. The initial basic flow is reduced to 0.9 of that in Fig. 2. The contour interval is the same as that in Fig. 1.

points, while $u_T$ and $v_T$ are the reference velocity fields which are related with (3-16b). We integrated the vorticity equation with a leapfrog time scheme for 14 days, which is the time required for the (5, 4) mode of the Rossby–Haurwitz wave to have one evolution without basic flow. One time step is taken as 540, 270, and 135 s for M16, M32, and M64, respectively.

To help understand the error growth with the basic flow slightly deviated from the stationary condition (3-16b), we first calculated the time evolution of (3-1) when the basic flow of superrotation is reduced to 0.9 of that in (3-16b). Figure 3 shows the stream function and zonal velocity with $\alpha = \pi/2 - 0.05$ at 64.5 h, at which time the error $L_2$ reaches 0.4. It is apparent that due to the weak basic flow the Rossby–Haurwitz wave travels in the direction opposite to that of the basic flow.

Figure 4 shows the error growth for M32, where the spherical-harmonics filter is used every $J_e$ time steps. Although the error $L_2$ grows with time exponentially, it remains $O(10^{-10})$–$O(10^{-12})$ at day 14. The errors are almost the same for $J_e = 30$ and 40 but increased by nearly 2 orders for $J_e = 50$. The error $L_3$ shows a similar time variation to $L_2$ but has a nearly 11 order smaller magnitude than $L_2$ at early stages. However, it can be seen that the difference between $L_2$ and $L_3$ decreases sharply with time for $J_e = 50$ beyond 4 days.

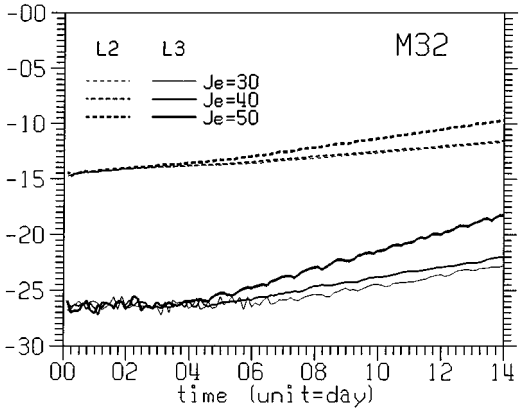


**FIG. 4.** Time variation of $\log_{10} L_2$ (in dashed lines) and $\log_{10} L_3$ (in solid lines) for $\alpha = \pi/2 - 0.05$ and M32. The spherical-harmonics filter is applied every $J_e$ time steps.

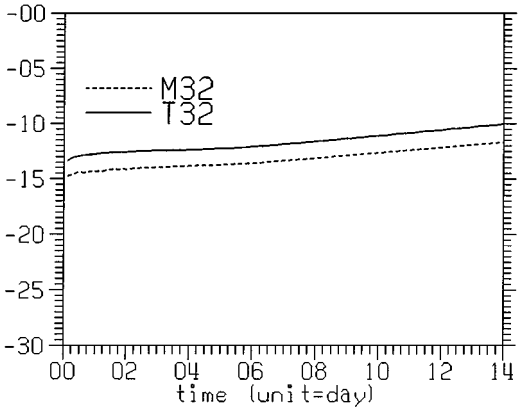


**FIG. 5.** Time variation of $\log_{10} L_2$ for M32 (dashed line) and T32 (solid line) with $\alpha = \pi/2 - 0.05$ and $J_e = 30$.

As might be expected, the error $L_2$ increases with the rotation angle with $J_e$ fixed, which was $0.36 \times 10^{-12}$ and $0.65 \times 10^{-12}$ for $\alpha = 0$ and $\alpha = \pi/4$, respectively ($0.23 \times 10^{-11}$ for $\alpha = \pi/2 - 0.05$ in Fig. 4), in the case of $J_e = 30$.

The quality of the results is tested by comparing them with those of the spherical-harmonics model [10, 19] of the same resolution, T32 having the total grid points of $K \times J = 128 \times 65$. For this resolution the maximum normality error of the Legendre functions is $2.3 \times 10^{-14}$ (cf. Jacob *et al.* [15]). One time step is taken as the same for M32, 270 s. The same Fourier filter as in (3-13) was used at every time step, too. We compare in Fig. 5 the error $L_2$ of M32 with $J_e = 30$ and T32. This shows that the result of M32 is more accurate than that of T32 by about $1\frac{1}{2}$ orders. Time variations of the errors for the two models are very similar. Both models exhibit an exponential error growth and the growth rate slightly increases after day 6 or so.

Figure 6 shows the effect of the model resolution, where the spherical-harmonics filter is used every 10, 30, and 60 time steps for M16, M32, and M64. At earlier stages the error increases as the model resolution becomes better, while this is reversed at later stages. At day 14, the error for M16 is about one order larger than that for M64.

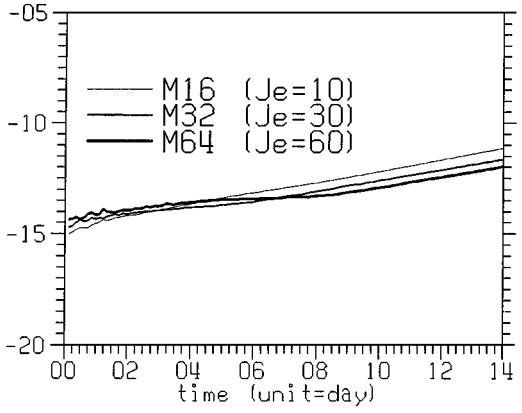


**FIG. 6.** Time variation of $\log_{10} L_2$ with $\alpha = \pi/2 - 0.05$ for various resolutions. The spherical-harmonics filter is applied every $J_e$ time steps.

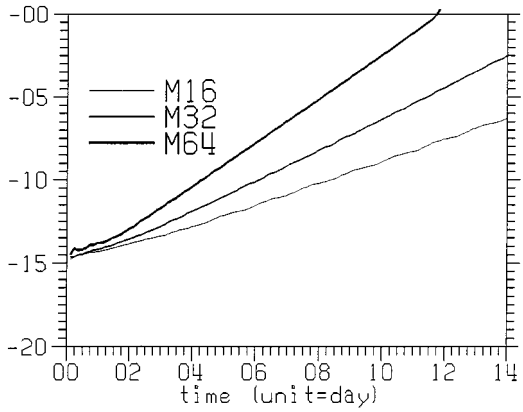


**FIG. 7.** Same as in Fig. 6 except that the spherical-harmonics filter is not applied.

In Fig. 7 we present the error growth when the spherical-harmonics filter is not used. It is noted that the error grows with time with a much larger growth rate than the cases where the spherical-harmonics filter is used. As the resolution becomes large, the growth rate also becomes large. For M64, the error reaches $O(1)$ at day 12 and the model encounters an overflow around day 13.

### 3.5. *Tests on the Advection of Cosine Bell*

In this section, we present the test with the advection of a scalar field, which is conserved following the motion. The equations used are the vorticity equation (3-1) and the advection equation

$$\frac{\partial h}{\partial t} = -\frac{U}{\sin^2\phi}\frac{\partial h}{\partial \lambda} - \frac{V}{\sin\phi}\frac{\partial h}{\partial \phi}, \tag{3-19}$$

where $h$ may be any scalar field. For a direct comparison with other results [15, 28], let $h$ be the geopotential height field scaled by $g/a\Omega^2$, with $g$ being the gravitational acceleration. The advective flow field of rigid rotation at $t = 0$ is given as

$$\zeta(\lambda', \theta') = \sin\theta'/6 \tag{3-20}$$

and is time-integrated by (3-1). The maximum flow speed is about 40 m/s, which gives one rotation of the scalar field during 12 days. The initial height field is given as the cosine-bell pattern [29], with its maximum value being 1000 geopotential meters in dimensional units.

Figure 8 shows the height field at various time stages and error fields after one rotation for $\alpha = \pi/2 - 0.05$ and M32. At day 12, the field of true solution is drawn in solid lines over the calculated pattern (dashed lines). Two contour lines are almost exactly overlapped so that we cannot visibly distinguish one from the other. The error field, having about 1% fluctuation, exhibits a nearly circular structure with the alternating sign, with greater amplitude over the cosine bell than over the outside region, which is common to other numerical methods as in [15, 28]. Not shown here is the fact that the amplitude of the error fluctuation is reduced to 0.24% at day 12 for M64.

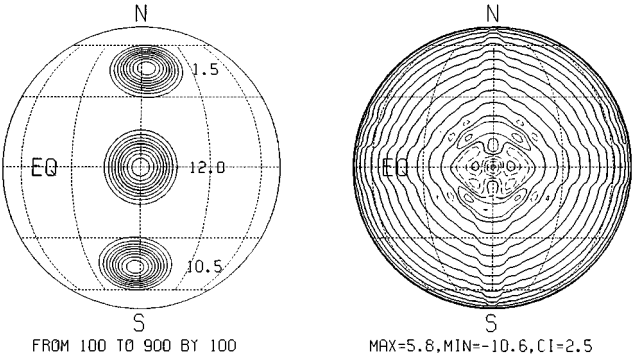


**FIG. 8.** (Left) Height field at days 1.5, 10.5, and 12 with $\alpha = \pi/2 - 0.05$. For day 12 the fields of exact solution (solid line) and calculation (dashed line) overlap. (Right) Height field error after one rotation (12 days).

Figure 9 shows the time variation of the normalized errors of hourly samples $L_1$, $L_2$, and $L_3$, defined as

$$L_1 = \frac{[|h - h_T|]}{[|h_T|]}$$
$$L_2 = \frac{\left[(h - h_T)^2\right]^{1/2}}{\left[h_T^2\right]^{1/2}} \qquad \text{(3-21a,b,c)}$$
$$L_3 = \frac{\max|(h - h_T)|}{\max|h_T|},$$

where $h_T$ denotes the true solution and the square bracket again means the global average. It is shown that the growth rate and magnitude of the error are very similar to one another

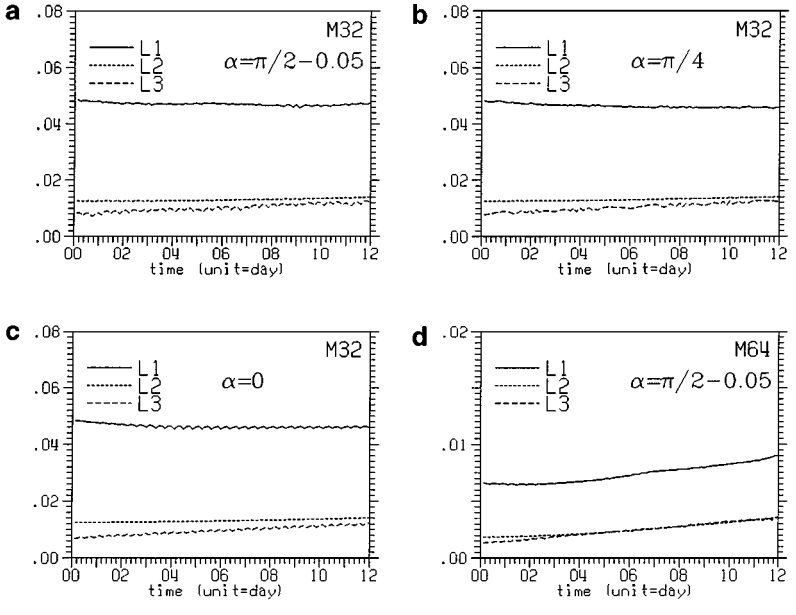


**FIG. 9.** Height error growth with time.

for $\alpha = \pi/2 - 0.05, \pi/4$, and 0. No significant signal of passing over the poles is seen from the error variation with time, which implies the absence of the so-called pole problem. It is of interest to note that the error $L_1$ decreases with time for M32 while it increases for M64. As in [15, 28], the curves are oscillating with time, reflecting the sampling errors on grid-point values.

Although precise comparison of the results with other methods is difficult because of different time-step sizes and resolutions, we give some comparisons for selected model parameters. For convenience, we compare our results for M32 to those of T42 for the spherical-harmonics model and $24 \times 16 \times 16$ for the spectral element model (for simplicity, referred to as SEM). The grid points of M32 and T42 are 8192, and SEM has 6144 grid points, while the time step sizes are 270, 1200, and 90 s, respectively. The $L_2$ errors at day 12 are 0.015, 0.04, and 0.02, where the rotation angle $\alpha$ is taken as $\pi/2 - 0.05$ for M32 and T42 and $\pi/2$ for SEM (the difference in $\alpha$ does not produce a significant change in errors). The error-growth rates (obtained by approximating the curves as a linear behavior) of $L_2$ for M32 and SEM are similar to each other, while $L_2$ error for T42 is at least five times larger than M32 and SEM due to large time step size [15].

## 4. DISCUSSION AND CONCLUSIONS

A new method for the solution of simple elliptic equations on a sphere by approximating the functions using truncated double Fourier series was presented with applications to the time-dependent nonlinear vorticity equation and advection equation. In addition to the advantages provided by Boer and Steinberg [2] and Yee [32], the present method gives a more definite and accurate formula because the constraint imposed on the spectral coefficients is not necessary, which can lead to increased accuracy and stability in a time-stepping procedure.

The solution of the Poisson equation was found to be more accurate than that by Yee's method for the even zonal wavenumbers other than zero, which comes from the use of basis functions satisfying the pole condition as in (2-5). The accuracy remains almost unchanged from Yee's [32] for odd zonal wavenumbers because the same basis functions are used, implying that taking the interior grids does not affect the accuracy for this problem. However, the difference in accuracy for zonal wavenumber zero still exists in spite of adopting the same basis functions when high resolution is used. If a function used for the test includes both even and odd zonal wavenumbers, the accuracy appears to be unchanged from Yee's because the improved accuracy for even zonal wavenumbers will be masked by odd zonal wavenumbers. It was shown that the error for the solution of biharmonic-type elliptic equations increases as the relative importance of the fourth order term increases. The accuracy drops by more than two orders compared to the Poisson equation when the relative magnitude of the fourth order term is one order larger than that of the second order term.

Through tests with the Rossby–Haurwitz wave of (5, 4) mode, which is stable [13], it was found that the new method can be applied successfully to the vorticity equation with high accuracy provided that the spherical-harmonics filter is used appropriately. The error measure defined in Eq. (3-18a) remains in the range from $O(10^{-11})$ for M16 to $O(10^{-12})$ for M64. To give a direct comparison with the reference solution, we time integrated the vorticity equation with the spherical-harmonics model using the same resolution (i.e., T32) and time-step size. The result showed that the present method is more accurate than the spherical-harmonics model by a factor of about $1\frac{1}{2}$ for the test used here.

Numerical integration without the spherical-harmonics filter was found to produce large errors compared to the results stated above. In particular, for M64 the error grows to $O(1)$ around day 12. The cure for this must be the spherical-harmonics filter, as was implied above. However, too frequent use of it deteriorates the efficiency coming from the use of double FFT. We confirmed that sufficiently less frequent use of it to keep the advantage of FFT works for test cases. Along with the advantage of double FFT, the present model can reduce the zonal grids near poles as in the spherical-harmonics model [12], while the shortcoming remains unavoidable that large storage is needed for the spherical-harmonics filter, which is comparable to that needed for the Legendre functions in the spherical-harmonics model.

Further application to the advection equation was carried out with one of the standard test method in [29]. Error measures for the strong advection of cosine bell with various rotation angles indicated that the present method is capable of producing accurate and stable calculations without the pole problem.

Test results as shown in Section 3 suggest that the double Fourier series used in this study could be applied to the numerical weather prediction model including shallow water equations without difficulty. We will present the test results with the standard test set proposed by [29] in the future.

## APPENDIX

The vorticity equation in flux form is written as

$$\frac{\partial \zeta}{\partial t} = -\frac{1}{\sin^2\phi}\frac{\partial}{\partial \lambda}(U\eta) - \frac{1}{\sin\phi}\frac{\partial}{\partial \phi}(V\eta), \tag{A-1}$$

with the definitions as in Section 3. Let $X_m(\phi, t)$ and $y_m(\phi, t)$ be the zonal Fourier transforms of $U\eta/\sin^2\phi$ and $V\eta$, respectively. Evaluation of the longitudinal advection term is straightforward. The $(n, m)$ component of latitudinal advection term for odd $m$ is calculated as

$$\begin{aligned}
&\frac{-1}{\pi}\int_0^\pi \frac{\sin n\phi}{\sin\phi}\left[\frac{\partial}{\partial\phi}y_m\right]d\phi \\
&\quad = \frac{-1}{\pi}\int_0^\pi y_m\left[\frac{n\cos n\phi}{\sin\phi} - \frac{\sin n\phi\cos\phi}{\sin^2\phi}\right]d\phi \\
&\quad = \frac{-1}{\pi}\int_0^\pi \frac{y_m}{2\sin^2\phi}[(n-1)\sin(n+1)\phi - (n+1)\sin(n-1)\phi]\,d\phi.
\end{aligned} \tag{A-2}$$

A similar expression for $m = 0$ may be obtained with ease. For even $m$ ($\neq 0$),

$$\begin{aligned}
&\frac{-1}{\pi}\int_0^\pi \frac{\sin n\phi}{\sin^2\phi}\left[\frac{\partial}{\partial\phi}y_m\right]d\phi \\
&\quad = \frac{-1}{\pi}\int_0^\pi y_m\left[\frac{n\cos n\phi}{\sin^2\phi} - \frac{2\sin n\phi\cos\phi}{\sin^3\phi}\right]d\phi \\
&\quad = \frac{-1}{\pi}\int_0^\pi \frac{y_m}{2\sin^3\phi}[(n-2)\sin(n+1)\phi - (n+2)\sin(n-1)\phi]\,d\phi.
\end{aligned} \tag{A-3}$$

Thus the spectral form of the vorticity equation is written as

$$\frac{d}{dt}\zeta_{n,m} = \begin{cases} -imX_{n,m} + \{(n-2)Y_{n+1,m} - (n+2)Y_{n-1,m}\}/2 & \text{for even } m\ (\neq 0) \\ -imX_{n,m} + \{(n-1)Y_{n+1,m} - (n+1)Y_{n-1,m}\}/2 & \text{for odd } m \text{ and } m = 0 \end{cases}$$

$$\frac{d}{dt}\zeta_{1,0} = -2Y_{0,0}, \qquad \text{(A-4a,b,c)}$$

where $X_{n,m}$ and $Y_{n,m}$ are the meridional transforms of $X_m(\phi, t)$ and $Y_m(\phi) \equiv y_m(\phi)/\sin^2\phi$, respectively. Truncation for $Y_{n,m}$ should be taken one level above that of $X_{n,m}$, and $Y_{-1,m}$ is discarded. In the derivation of spectral form for the latitudinal advection term, we used the fact that $V\eta/\sin^2\phi$ must be bounded at poles.

Since from (A-1) the global integral of the vorticity is conserved with time, the spectral equations (A-4) should also satisfy this conservation property. Using Eq. (3-10),

$$\begin{aligned} \frac{d}{dt}[\zeta] &= \frac{d}{dt}\sum_{\substack{n=0 \\ \text{even}}}^{N} \frac{\zeta_{n,0}}{1-n^2} \\ &= -\frac{1}{2}Y_{1,0} + \frac{1}{2}\sum_{\substack{n=2 \\ \text{even}}}^{N} \frac{1}{1-n^2}\{(n-1)Y_{n+1,0} - (n+1)Y_{n-1,0}\} \\ &= -\frac{1}{2(N+1)}Y_{N+1,0}; \end{aligned} \qquad \text{(A-5)}$$

thus we must discard $Y_{N+1,0}$ to meet the vorticity conservation in the absence of forcing and dissipation. Time integration with (A-4) showed that the error for Rossby–Haurwitz waves tested is larger than that resulting from the time integration with (3-8) by nearly $O(10^3)$.

## ACKNOWLEDGMENTS

The author acknowledges the financial support of the Korea Research Foundation made in the program year 1997. He also thanks the anonymous reviewers for their constructive comments. He thanks members of the atmospheric modeling laboratory in Pukyong National University, D.-K. Shin, Y.-C. Song, M.-K. Kang, and T.-Y. Goo, for their support and helpful discussions.

## REFERENCES

1. S. R. M. Barros, Multigrid methods for two- and three-dimensional Poisson-type equations on the sphere, *J. Comput. Phys.* **92**, 313 (1991).
2. G. J. Boer and L. Steinberg, Fourier series on spheres, *Atmosphere* **13**, 180 (1975).
3. W. Bourke, An efficient, one-level, primitive-equation spectral model, *Mon. Weather Rev.* **100**, 683 (1972).
4. J. P. Boyd, The choice of spectral functions on a sphere for boundary and eigenvalue problems: A comparison of Chebyshev, Fourier and associated Legendre expansions, *Mon. Weather Rev.* **106**, 1184 (1978).
5. J. P. Boyd, Chebyshev and Fourier spectral methods, in Lecture Notes in Engineering, edited by C. A. Brebbia and S. A. Orszag (Springer-Verlag, New York, 1989).
6. S. C. Dennis and L. Quartapelle, Spectral algorithms for vector elliptic equations in a spherical gap, *J. Comput. Phys.* **61**, 218 (1985).
7. G. A. Dilts, Computation of spherical harmonic expansion coefficients via FFT's, *J. Comput. Phys.* **57**, 439 (1985).

8. M. Elowitz, F. Hill, and T. L. Duvall, A test of a modified algorithm for computing spherical harmonic expansion coefficients using an FFT, *J. Comput. Phys.* **80**, 506 (1989).
9. W. L. Gates, The atmospheric model intercomparison project, *Bull. Amer. Meteor. Soc.* **73**, 1962 (1992).
10. G. J. Haltiner and R. T. Williams, *Numerical Weather Prediction and Dynamic Meteorology* (Wiley, New York, 1980), 2nd ed.
11. B. Haurwitz, The motion of atmospheric disturbances on the spherical earth, *J. Mar. Res. III* **3**, 255 (1940).
12. M. Hortal and A. J. Simmons, Use of reduced Gaussian grids in spectral models, *Mon. Weather, Rev.* **119**, 1057 (1991).
13. D. J. Hoskins, Stability of the Rossby–Haurwitz wave, *Quart. J. Roy. Meteor. Soc.* **99**, 723 (1973).
14. D. J. Hoskins and A. J. Simmons, A multi-layer spectral model and the semi-implicit method, *Quart. J. Roy. Meteor. Soc.* **101**, 637 (1975).
15. R. Jacob, J. Hack, and D. L. Williamson, Spectral transform solutions to the shallow water test set, *J. Comput. Phys.* **119**, 164 (1995).
16. M. N. Jukes and M. E. McIntyre, A high-resolution one-layer model of breaking planetary waves in the stratosphere, *Nature* **328**, 590 (1987).
17. P. E. Merilees, The pseudospectral approximation applied to the shallow water equations on a sphere, *Atmosphere* **11**, 13 (1973).
18. S. Moorthi and R. Y. Higgins, Application of Fast Fourier Transform to the direct solution of a class of two-dimensional separable elliptic equations on the sphere, *Mon. Weather Rev.* **121**, 290 (1993).
19. T. Nehrkorn, On the computation of Legendre functions in spectral models, *Mon. Weather Rev.* **118**, 2248 (1990).
20. S. A. Orszag, Transform method for the calculation of vector-coupled sums: Application to the spectral form of the vorticity equation, *J. Atmos. Sci.* **27**, 890 (1970).
21. S. A. Orszag, Fourier series on spheres, *Mon. Weather Rev.* **102**, 56 (1974).
22. W. H. Press, S. A. Teukolsky, W. T. Vettering, and B. P. Flannery, *Numerical Recipes* (Cambridge Univ. Press, Cambridge, UK, 1992).
23. A. J. Robert, The integration of a low order spectral form of the primitive meteorological equations, *J. Meteor. Soc. Jpn.* **44**, 237 (1966).
24. W. F. Spotz, M. A. Taylor, and P. N. Swartztrauber, Fast shallow-water equations solvers in latitude-longitude coordinates, *J. Comput. Phys.* **145**, 432 (1998).
25. P. N. Swartztrauber, The direct solution of the discrete Poisson equation on the surface of a sphere, *J. Comput. Phys.* **15**, 46 (1974).
26. P. N. Swartztrauber, On the spectral approximation of discrete scalar and vector functions on the sphere, *SIAM J. Numer. Anal.* **16**, 934 (1979).
27. P. N. Swartztrauber, Spectral transform methods for solving the shallow-water equations on the sphere, *Mon. Weather Rev.* **124**, 730 (1996).
28. M. Taylor, J. Tribbia, and M. Iskandarani. The spectral element method for the shallow water equations on the sphere, *J. Comput. Phys.* **130**, 92 (1997).
29. D. L. Williamson, J. B. Drake, J. J. Hack, R. Jakob, and P. N. Swartztrauber, A standard test set for numerical approximations to the shallow water equations in spherical geometry, *J. Comput. Phys.* **102**, 211 (1992).
30. S. Wolfram, *Mathematica* (Wolfram Research, Champaign, IL, 1988).
31. S. Y. K. Yee, Studies on Fourier series on spheres, *Mon. Weather Rev.* **108**, 676 (1980).
32. S. Y. K. Yee, Solution of Poisson's equation on a sphere by truncated double Fourier series, *Mon. Weather Rev.* **109**, 501 (1981).